Building Large Amorphous Polymer Structures: Atomistic Simulation of Glassy Polystyrene

M. Kotelyanskii,† N. J. Wagner, and M. E. Paulaitis*

Center for Molecular and Engineering Thermodynamics, Department of Chemical Engineering, University of Delaware, Newark, Delaware 19716

Received January 16, 1996; Revised Manuscript Received July 12, 1996[⊗]

ABSTRACT: A technique is presented for generating atomistic models of amorphous polymer structures starting from chain configurations on lattice. The method guarantees Gaussian chain statistics and enables control of chain tacticity and monomer sequence while avoiding severe overlaps between the atoms in the structure. We show that the single polymer chain, which completely occupies the lattice with periodic boundary conditions, is Gaussian with chain statistics equivalent to that obtained for a nonreversing random walk on the cubic lattice. The method enables efficient generation of the chain topology, which can then be populated with specific chemical units. Large models of glassy, atactic polystyrene have been generated, and the effects of system size are examined in terms of calculated X-ray scattering intensities. These results demonstrate the efficacy of this new method for generating more realistic polymer glass structures.

I. Introduction

Computer simulations using Monte Carlo or molecular dynamics (MD) techniques have proven to be a powerful tool for studying the molecular structure and dynamics of solids and liquids.[1,2] However, as glasses are inherently nonergodic, nonequilibrium structures, generating representative glass structures computationally is nontrivial. Generating polymer chains directly by propagating the chain in the simulation box is possible only for densities well below the experimental densities of polymer melts or glasses.[3] A number of methods for generating polymer glass structures have recently been proposed. The technique most widely used is based on packing a chain configuration, generated in vacuum, into a periodic box.[4] An alternative technique[5] starts by randomly placing the monomer in the periodic box and then "polymerizing" the monomers to form the chain.

Both techniques have advantages and disadvantages. The first approach allows a desired monomer sequence along the polymer chain, tacticity, and correct chain statistics to be specified as long as the initial chain configuration is constructed using rotational isomeric states,[6] but it suffers from severe atomic overlaps in the initial stages of relaxing the structure. The overlaps lead to large repulsive forces between atoms, requiring a special multistep treatment with reduced atomic radii. This method becomes more difficult to implement as the chemical structure of the repeat unit becomes more complex.[7−9] Furthermore, only chain configurations that pack into the periodic box are selected, which potentially can influence the chain statistics.

The problem of severe overlaps is avoided in the second approach[5] by starting with the monomer liquid before "polymerization". However, introducing chemical bonds between the monomers results in highly strained bond lengths and valence angles, which require several stages of minimization and annealing to relax the resulting chain structure. Nevertheless, unlike repulsive interatomic potentials, bond length and valence angle potentials are stiff but harmonic; thus, large deviations in bond lengths and angles appearing in the initial guess structure result in large but still manageable forces. The statistics of the chain are, however, not guaranteed in this approach, and further complications arise when it becomes necessary to specify a desired monomer sequence or tacticity.[5]

In this article, we describe an alternative approach for generating polymer chains that avoids severe overlaps, guarantees Gaussian chain statistics, and enables control over monomer sequence and tacticity. The idea is to start with a trajectory generated by a self-avoiding walk on the completely occupied cubic lattice. This trajectory becomes the chain backbone, which is then decorated by atoms according to the specific chemical structure of the polymer. Initial lattice chain configurations are generated using a modification of the algorithm proposed by Pakula and Geyler.[10] We demonstrate that these lattice chains obey Gaussian statistics necessary for generating configurations in the melt[11] with a persistence length equal to that of the nonreversing random walk. The similarity between self-avoiding and nonreversing random walks has been observed previously in the lattice simulation of concentrated polymer systems.[12] Thus, the algorithm produces a single lattice chain that both fills the lattice and satisfies periodic boundary conditions similar to the atomistic parent chain in ref 4.

To generate the atomistic polymer, lattice sites connected along the chain contour are sequentially populated with building blocks containing the atoms of the monomer unit. Proper placement and orientation of atoms within the block simultaneously avoids overlaps and minimizes, to some extent, distortions in bond lengths and valence angles. The sequence in which blocks are placed on the lattice and the contents of the blocks define the monomer sequence and tacticity. Subsequent relaxation of this structure is possible with only one stage of energy minimization using the full potential parameters. Further annealing by MD removes the lattice periodicity and generates structures that reproduce experimental X-ray scattering patterns.

As an illustration, we apply the method to study amorphous atactic polystyrene. This polymer is widely used commercially, and its structure has been studied extensively by a variety of methods, including both computer simulation[5,7,13] and different scattering techniques.[14−18] Thus, it is an ideal test case. Polystyrene also possesses an interesting feature in its scattering pattern, known as the "polymerization peak", the

† Current address: Department of Materials Science and Engineering, The Pennsylvania State University, University Park, PA 16802.

[⊗] Abstract published in *Advance ACS Abstracts,* December 1, 1996.

S0024-9297(96)00071-X CCC: $12.00

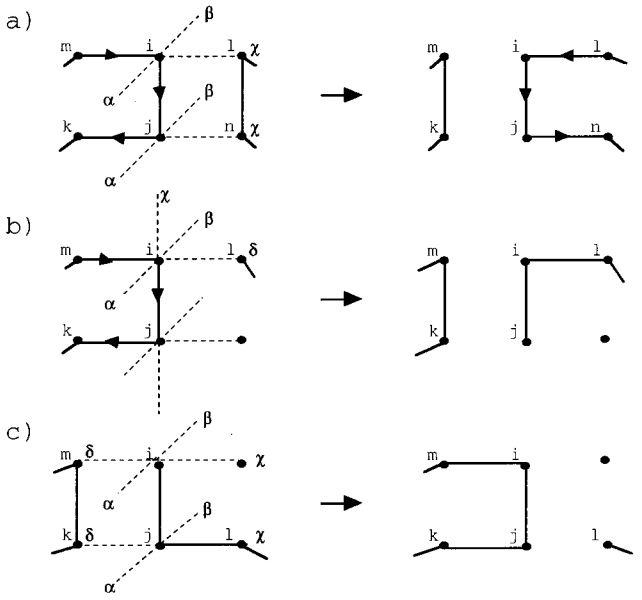

Figure 1. Different types of moves implemented to move a chain on the lattice: (a) "kink + bond", (b) "kink + end", and (c) "end + bond".

origin of which is not understood. To demonstrate the efficiency of our new method for studying large system sizes, we generate several realizations of atactic polystyrene structure of different sizes at the experimentally observed density at 300 K. X-ray scattering patterns of these different structures are then calculated and analyzed to elucidate system size effects.

II. Building a Periodic Gaussian Chain on the Cubic Lattice

A. Self-Avoiding Chains on the Completely Occupied Lattice. Lattice computer simulations of idealized polymers have proven to be helpful in themselves in elucidating fundamental properties of polymer chains, such as scaling laws describing chain geometry[19−21] or phase transitions in polymer mixtures[22,23] and dense polymer melts.[24] Different algorithms for simulating motions of polymer chains on lattices have been suggested (*e.g.*, see refs 25 and 26 and references therein). However, most algorithms can be applied only when empty lattice sites are available and ultimately fail on the completely occupied lattice. Methods to overcome this problem have been proposed.[10,26−28] Some involve "chemical reactions" to break and reconnect chains on the lattice,[26−29] which is acceptable for multiple chain systems if the chain length distribution is properly monitored.[27] However, this method is not efficient for generating a single chain or a few long chains on a large lattice.

As described above, an alternative solution is to generate single Gaussian chains that occupy all the lattice sites and then select only those that fold into the periodic box. A similar approach, introduced by Theodorou and Suter,[4] is often used for off-lattice atomistic simulations of amorphous polymers in order to minimize the effect of chain ends.[3,8,9]

To efficiently generate Gaussian chains that both fill space and satisfy periodic boundary conditions, we employ a technique based on a method proposed by Pakula and Geyler.[10] In this method, the lattice is arbitrarily filled by chains and then "annealed" by a Monte Carlo-type algorithm in which chain motions are implemented through the "kink + bond" move (Figure 1a). This move involves the interaction between a kink in the chain and a neighboring bond parallel to the kink on the lattice, such that the kink is propagated along the lattice. This move corresponds to "reptation" of the chain by two chain segments between the bond and the kink. Additional "kink + end" and "end + bond" moves (Figure 1b and c, respectively) involve propagating the chain end when a kink or a bond parallel to it is nearby. These moves are essential for the ergodicity of the algorithm as they create, remove, or reorient kinks and change the positions of chain ends. The ergodicity of lattice simulations, employing different kinds of reptation moves, has been verified elsewhere.[29]

Our version of Pakula and Geyler's algorithm proceeds as follows. An initial chain configuration is placed on the lattice, with each lattice site numbered according to its position along the chain backbone. To effect a move, a lattice site i (see Figure 1) is chosen at random, and the lattice positions of its two neighbors along the chain are determined. If site i is a chain end, an attempt to make an end + bond move is made. If site i is not one of the chain ends, then a determination is made to identify it as part of a kink. For example, in Figure 1a, if sites m and k are separated by one lattice spacing, then the three bonds connecting sites m, i, j, and k must form a kink. If site i is part of a kink, then either a kink + bond or a kink + end move is attempted. As shown below, the kink + end move must be chosen with a probability of $^1/_2$ to ensure that the probabilities of any move and its reverse are equal, which assures detailed balance.

If the kink + bond move is attempted, one of the three adjacent sites marked α, β, or χ (see Figure 1a) is selected at random to find a bond parallel to i−j. If no bond is located, the move ends unsuccessfully. If a parallel bond is located, the nodes are reconnected, such that the new bonds m−k, l−i, and n−j are created, and bond l−n is broken (Figure 1a).

If the kink + end move is attempted (Figure 1b), then either site i or j is selected at random with equal probability and checked to determine if a chain end is a nearest neighbor. For instance, if site i was chosen, then nodes α, β, χ, and δ are checked. If a chain end is found (*e.g.*, site δ), then bonds l−i and m−k are created, and bonds m−i and k−j are broken.

The end + bond move (Figure 1c) is just the reverse of the kink + end move. If site i is found to be a chain end, the end + bond move is selected with a probability of $^1/_4$ (see below). To proceed, the site connected to site i is located to identify bond i−j in Figure 1c, and one of the four possibilities for an adjacent, parallel bond is checked at random. If one is found (bond m−k in the same figure), the sites are reconnected such that kink m−i−j−k is created, and the chain end is moved to site l.

As shown below, the scheme described above assures detailed balance; therefore, all self-avoiding chain configurations completely filling the lattice are sampled with the same probability. For the kink + bond move, both forward and reverse moves are made in the same manner and with equal probability. For the kink + end move, the probability of the forward move (left to right in Figure 1b) is

$$P_+ = (\text{probability of attempting kink + end move}) \times (\text{probability of choosing site i from either site i or j}) \times (\text{probability of choosing the adjacent site l})$$

$$= (^1/_2)(^1/_2)(^1/_4) = {}^1/_{16}$$

The probability of the reverse move (right to left in Figure 1b) is the same as the forward (left to right) end + bond move in Figure 1c:

$$P_- = (\text{probability of attempting the end + bond move}) \times (\text{probability of finding m−k bond})$$

$$= (^1/_4)(^1/_4) = {}^1/_{16}$$

In a system consisting of multiple chains, these moves will result in a distribution of chain lengths. For a single chain, these moves correspond to reptations of portions of the chain along its backbone. Thus, the search for "mobile loops" necessary to keep the original chain lengths in multiple chain systems[10] is not necessary here. This simplification makes the modified algorithm "local", as any move involves only neighboring sites, and thereby simplifies its parallel implementation on distributed memory parallel computers or workstation clusters.

Typically 10^3−10^4 Monte Carlo cycles per lattice site were found to be sufficient to "anneal" the initial guess to the Gaussian chain. A Monte Carlo cycle for a cubic $N \times N \times N$ lattice and a $(N^3 - 1)$ chain length consists of N^3 attempts

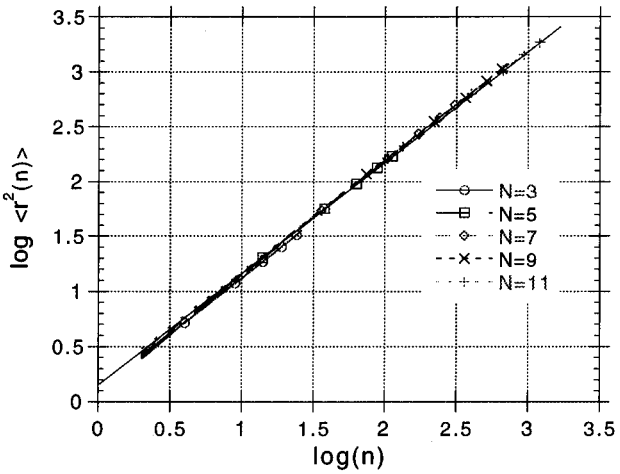

Figure 2. Mean-squared length of the vector connecting chain head with the segment number n along the chain path as a function of n for different lattice sizes and chain lengths, $N^3 - 1$, with $N = 3$, 5, 7, 9, and 11.

to make a move. The algorithm required 4.7 s of CPU time for $N = 5$ and 118 s of CPU time for $N = 11$ to complete 1000 cycles on a scalar IBM RISC 6000/590 workstation.

At this point, we have described an algorithm for generating single chain configurations on a completely occupied lattice without intersections, which also satisfies periodic boundary conditions. It has been shown previously[10] that chains of length N on the cubic $N \times N \times N$ lattice obey Gaussian statistics. We demonstrate that this also holds true for a single chain with $(N^3 - 1)$ bonds folded into the $N \times N \times N$ lattice with periodic boundary conditions. A plot of the logarithm of the mean-squared magnitude of the vector separating lattice sites connected by n bonds along the chain is shown in Figure 2 as a function of $\log(n)$ for different periodic lattice sizes and corresponding chain lengths ($N^3 - 1$), with $N = 3$, 5, 7, 9, and 11. The slopes of these lines are all equal to 1, showing that the chains are, indeed, Gaussian with $\langle r^2(n)\rangle = An$, and $A = 1.48 \pm 0.04$ from the intersection of the best fit line with the ordinate. This result is in agreement with previous results,[10,27] and demonstrates that neither the power law nor the persistence length, A, depends on the system size.

B. Comparison of Self-Avoiding and Non-Self-Avoiding Random Walks. According to the Flory's theorem,[11] chain statistics in the melt will be equivalent to the non-self-avoiding chain. A simple random walk on the cubic lattice obeys Gaussian statistics with a persistence length $A = 1$. Our algorithm, however, follows the nonreversing random walk on the cubic lattice, in which the walker proceeds onto any of the neighboring lattice sites except the one visited on the preceding step. The mean-squared distance separating the position at step i from that at step $(i + k)$ can be written as a function of k as

$$\langle(\vec{r}_{(i+k)} - \vec{r}_i)^2\rangle = (k-1)(1 + 2\sum_{p=1}^{k-1}\langle(\vec{u}_0 \cdot \vec{u}_p)\rangle) \qquad (1)$$

where $r_{(i+k)}$ and $r_{(i)}$ are the positions at the $(i + k)$th and the ith step, respectively, and $\vec{u}_p$ is the displacement vector for step p. The lattice spacing, or equivalently the length of $\vec{u}_p$, is equal to unity. If the probability of turning in any direction is equal, then from symmetry considerations, it is apparent that the only non-zero contributions to the sum over p steps in eq 1 comes from sequences of straight-ahead moves. If the probability of moving forward at each step is P, then the probability of such a sequence occurring is P^m, where m is the number of straight-ahead moves. The sum over p steps in eq 1 is then the sum of the geometric sequence, which in the limit of large k yields

$$\langle(\vec{r}_{(i+k)} - \vec{r}_i)^2\rangle = k(1 + 2P/(1 - P)) \qquad (2)$$

If the probability of moving in any one of the allowed directions is the same, then $P = 1/5$, and

$$\langle(\vec{r}_{(i+k)} - \vec{r}_i)^2\rangle = 1.5k \qquad (3)$$

which results in the scaling law obtained for the self-avoiding chain on a completely occupied lattice.

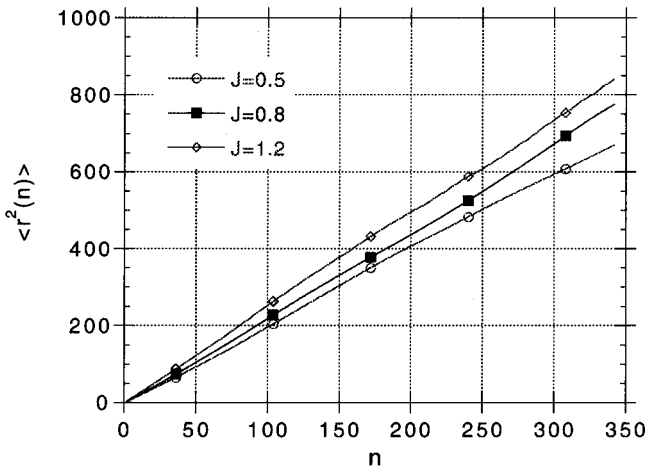

Figure 3. Mean-squared length of the vector connecting chain end with the segment number n along the chain path for "biased" self-avoiding walks on a $7 \times 7 \times 7$ lattice as a function of n for different values of J (see eq 5).

C. Constructing Self-Avoiding Lattice Chains with Different Persistence Lengths. The above argument suggests a simple algorithm for constructing self-avoiding chains on the completely occupied lattice with a persistence length different from 1.5. By assigning zero energy to each turn and an energy of $-J$ to each step that continues straight ahead, one can generate a biased random walk with a probability of moving straight ahead different from that for turning. This algorithm mimics a polymer chain with a bond rotation potential.[6] For the nonreversing random walk, the probability of moving forward will then be

$$P = \exp(-J)/(4 + \exp(-J)) = 1/(1 + 4\exp(J)) \qquad (4)$$

Consequently, the persistence length becomes

$$A = 1 + 0.5\exp(J) \qquad (5)$$

To test this algorithm, the nonreversing random walk on a cubic lattice was simulated with these weighted probabilities. A number of self-avoiding chains were also generated by our modified Pakula algorithm, with an acceptance probability given by the Metropolis sampling criterion.[2] That is, if the energy of the new configuration is lower than that of the original configuration, the rearrangement is always accepted, whereas if the energy of this configuration is higher, it is accepted with the probability of the inverse exponent of the corresponding energy change.

Results for self-avoiding random walks on a cubic $7 \times 7 \times 7$ lattice (Figure 3) show that the biased self-avoiding chain remains Gaussian, and, as expected, its persistence length increases with increasing J. Figure 4 presents persistence lengths for different values of J obtained from the nonreversing and self-avoiding random walks on the same cubic lattice and calculated from eq 5. Note that $A = 1.5$ at $J = 0$, in accordance with the results for the nonbiased self-avoiding walk. Results for the nonreversing walk agree perfectly with eq 5, and the self-avoiding chain follows the calculated curve to within the accuracy of our simulation. Biasing makes the kink configurations less favorable, which makes the simulation less efficient, as kinks are the main "locomotives" for chain configuration changes. This results in slower convergence and the larger uncertainties in Figure 3 for the self-avoiding walk, as more Monte Carlo cycles are required to produce uncorrelated configurations.

III. Building Atomistic Models of Amorphous Polymer

The trajectory of the self-avoiding walk generated on the cubic lattice must be mapped onto another self-

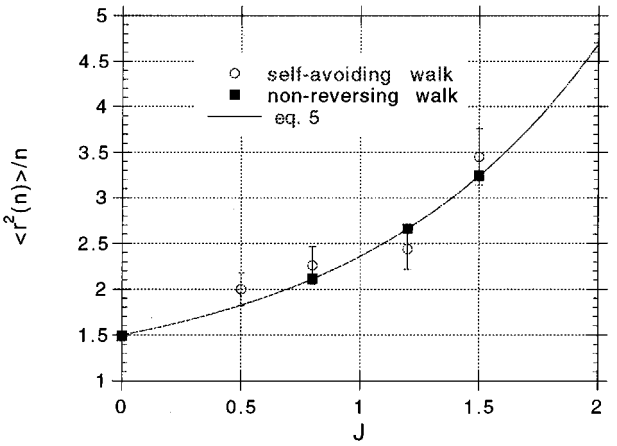

Figure 4. Persistence length for biased self-avoiding (circles) and nonreversing (squares) random walks.

avoiding walk for the atomistic polymer chain. Two parameters must be specified to yield the desired polymer chain. The first is the unit of physical length in space, which we assign to one bond length on the lattice (*i.e.*, lattice spacing, l_l), and the second is the number of atomistic monomers assigned to one lattice bond, n. As stated above, we assume that the actual polymer chain in the melt or the glass obeys Gaussian statistics. That is, its average end-to-end distance is proportional to the square root of its length, N_l. The coefficient of this proportionality is $C_{inf} = \langle \Delta r^2(N_l) \rangle / N_l a^2$,[6] where a is the length of one monomer along the chain contour and C_{inf} is a parameter characteristic of the polymer chemical structure. This characteristic parameter has values between 4 and 11 for the most common polymers.[6] For a lattice of N_l sites, the mean-squared end-to-end distances are

$$\langle \Delta r^2 \rangle_{lattice} = 1.5 l_l^2 N_l \tag{6}$$

$$\langle \Delta r^2 \rangle_{polymer} = C_{inf} a^2 N_l n \tag{7}$$

which gives

$$l_l^2 = C_{inf} a^2 n / 1.5 \tag{8}$$

The chain must also pack into the periodic box with a prescribed density. Equating the lattice volume, $N_l l_l^3$, to the volume of the chain, $N_l n v_0$, where v_0 is the volume per monomer, we obtain

$$l_l^3 = n v_0 \tag{9}$$

From eqs 8 and 9,

$$l_l = \alpha \beta a \tag{10}$$

$$n = \alpha^3 \beta^2 \tag{11}$$

where we have introduced the two dimensionless parameters,

$$\alpha = 1.5 / C_{inf} \tag{12}$$

$$\beta = v_0 / a^3 \tag{13}$$

such that α describes the flexibility of the polymer relative to the self-avoiding walk on the cubic lattice, and β characterizes the shape of the monomer unit.

To illustrate the method described above, glassy amorphous atactic polystyrene chains have been constructed. Based on the chemical structure of the polystyrene monomer, the length of one repeat unit is calculated to be $a = 2.56$ Å (i.e., the distance between two chiral carbons on adjacent monomers). If we assume that the experimental density of polystyrene at 300 K is 1.02 g/cm^3, the volume per monomer is $v_0 = 164$ Å^3. In addition, $C_{inf} = 8.6$ for atactic polystyrene with 50% meso diads.[7] Using eqs 8−13, these parameters give one monomer per two lattice sites ($n = 0.5$), with $l_l = 4.374$ Å.

The AMBER 4.1 simulation package, modified to support periodic boundary conditions via the minimum image convention, was used to perform potential energy minimizations and MD simulations. The nonbonded and intramolecular potential parameters were taken directly from the AMBER force-field database.[30] Partial charges were assigned on the basis of semiempirical AM1 calculations as in ref 5. The following single chain amorphous structures, having an average fraction of meso diads equal to 0.5, were generated from the chain configurations on $5 \times 5 \times 5$, $7 \times 7 \times 7$, and $9 \times 9 \times 9$ lattices: four 62-mers [(21.75 Å)^3 cube], three 171-mers [(30.625 Å)^3 cube], and two 364-mers [(39.15 Å)^3 cube], respectively. Lattice chain configurations used to generate different atomistic realizations were separated by 10^5 Monte Carlo cycles.

The main concern when placing atomistic monomers on the lattice chain is to minimize nonbonded overlaps between the atoms. This is achieved by preparing "building blocks" containing the group of polymer atoms assigned to one lattice site. These building blocks are then placed on the lattice sites and oriented by taking into account the group orientation with respect to its two nearest neighbors along the chain. For polystyrene, the building block is a cube with $l_l = 4.374$ Å, and two building blocks define the polymer: one contains the chiral carbon, the phenylene ring, and pendant hydrogen; the other contains the methylene group (Figure 5). Each building block has its own internal frame of reference, so that atoms within the block can be placed onto a lattice site with proper orientation of the chain backbone and the bulky phenylene ring. The center of the building block is located on the lattice site, and its internal z-axis is pointed in the direction of the next lattice site along the chain backbone. The internal y-axis is oriented such that atoms to be connected by a chemical bond (aliphatic carbons in this case) are not separated from each other by a phenylene ring. The desired fraction of meso diads is set by applying the mirror symmetry transformation with respect to the internal yz-plane for atoms in the building block containing chiral carbons. For the atactic polymer, random numbers are drawn to decide whether this transformation is applied or not. Chirality does not change during the subsequent stages of structure optimization and annealing. The internal coordinates of the atoms belonging to the building blocks are then transformed into the laboratory frame of reference.

In general, bond lengths and angles in this initial structure are far from their equilibrium values, and some overlaps between the atoms are still possible. However, due to precautions taken in the previous steps, the energy drops rapidly to values corresponding to room temperature averages after fewer than 1000 steps of conjugate gradient minimization using the full Lennard-Jones parameters. To assure that the structure is completely relaxed, several thousand conjugate gradient minimization steps are performed, which drops the maximum gradient to 10^{-1} kcal mol^{-1} Å^{-1}. Every initial structure produced by this algorithm was readily minimized using the full potentials without complicated

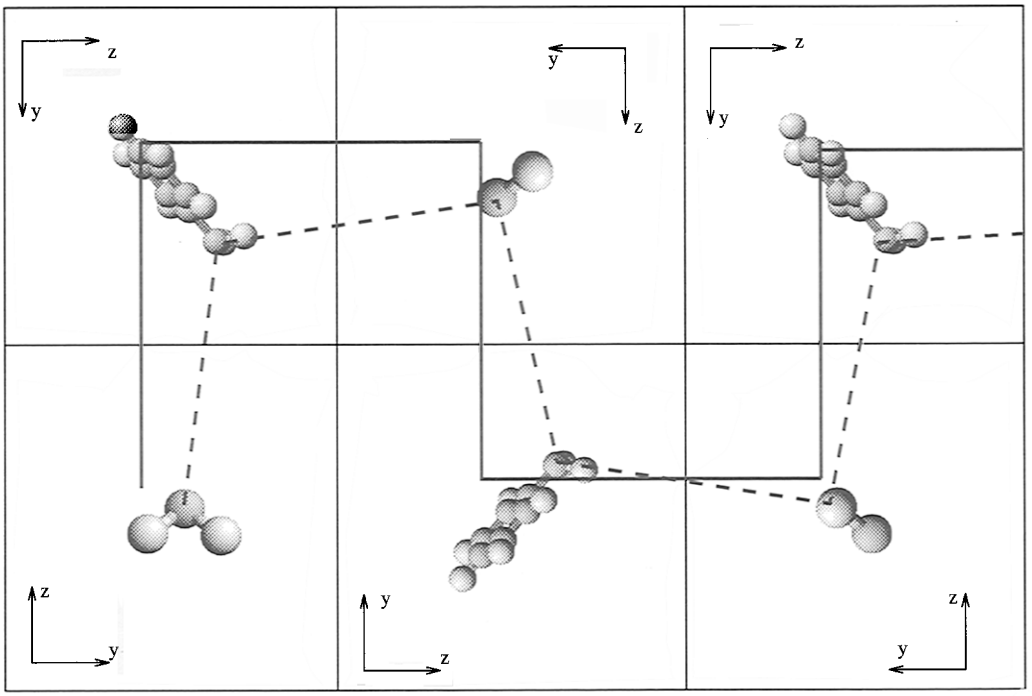

Figure 5. Two types of "building blocks" used to build polystyrene glass and their placement on the lattice chain. The thick solid line shows the lattice chain path; dashed lines represent the backbone bonds to be created and optimized during the minimization step. Axes show the orientation of the local reference frame of each block.

multistage procedures involving shrinking or expanding the van der Waals radii. As the main purpose of this step is to remove any overlaps and to fix the chain geometry, we save computational effort by using a short cutoff of 4 Å for all the nonbonded interactions. This was followed by an annealing MD run at 1000 K, also with a cutoff of 4 Å. The bond length deviations following minimization were small enough to allow us to maintain all the bond lengths constant using the SHAKE algorithm[31] immediately after energy minimization. We used SHAKE during the high-temperature annealing and the 300 K MD runs, with a maximum allowed deviation in the bond length of 0.01 Å. Finally, all structures were annealed at 300 K with 9 Å cutoff and time step of 2 fs. The last 100 ps of these runs was used to calculate X-ray scattering patterns. Two sets of final structures with different cooling histories were produced. Set A consists of four 62-mers, three 171-mers, and two 364-mers annealed for 100 ps at 1000 K and 200 ps at 300 K. Set B was produced from the same minimized initial configurations but annealed for 200 ps at 1000 K and for 100 ps at 300 K. All MD runs were performed at constant density.

IV. Results and Discussion

Table 1 presents potential energy contributions and chain end-to-end distances after energy minimization (step 0), 100 ps of molecular dynamics at 1000 K (step 1), and 200 ps of molecular dynamics at 300 K (step 2). For comparison, we also present results for a liquid of 364 styrene monomer molecules, generated using the same method and the same initial lattice configuration as the second 364-mer, but without connecting monomers to each other. The initial configuration of this system has a relatively high energy (13 259 kcal/mol per molecule), but, as expected, the liquid relaxes faster than the polymer. Contributions to the potential energy at the end of each step of annealing are quite close for structures of different size, as well as between the polymer and monomer systems. Thus, the structures generated by this method are free from unrealistically large bond length and valence angle distortions or atomic overlaps.

We define the end-to-end distance as the separation between the first and the last atoms of the unfolded chain. The change in end-to-end distance during the simulations did not exceed the size of the monomer unit (about 7 Å), which can be accounted for by simple rotation of the segments without invoking major changes in the chain backbone configuration. This is illustrated by Figure 6, which shows configurations of one 62-mer immediately following "decoration" of the lattice (Figure 6a), potential energy minimization (Figure 6b), and 100 ps MD run at 1000 K (Figure 6c).

The chain conformation statistics obtained from our simulations at 300 K are similar to those obtained by Khare *et al.*[5] Average populations of the different conformational states are given in Table 2. The definition of torsion angles and rotational isomeric states for meso and racemo diads are the same as in ref 5, which in turn follows Flory's definition.[6]

Comparison of our generated polystyrene structures with the extensive results of X-ray scattering studies[14,17,32] provides a more comprehensive test of how realistic our structures are. Further, the calculated scattering patterns are sensitive to any periodicity in the structure and, therefore, can be used to check for the presence of residual lattice periodicity in the final amorphous structures.

X-ray scattering intensities in electron units per carbon atom were calculated from the Fourier transform of the density, weighted by the appropriate atomic scattering factors:[16]

$$\rho(\vec{q}) = \sum_{j=1}^{M} \exp(i\vec{r}_j\vec{q})\, f_j(q) \tag{14}$$

$$I(q) = \langle \rho(\vec{q})^* \rho(\vec{q}) \rangle / N_C \tag{15}$$

where M is the total number of atoms in the system, N_C is the number of carbon atoms, $\vec{q}$ is a scattering

Table 1. Potential Energy and End-to-End Distance Values Obtained at the End of Different Stages of the Polystyrene Structures Preparation[a]

chain length	structure no.	step	potential energy	nonbonded energy	bond angle energy	bond energy	end-to-end distance (Å)
62	1	0	−0.12	−9.50	2.56	0.58	52.03
62	1	1	26.89	−6.94	18.56	0.01	47.73
62	1	2	0.68	−10.56	5.50	0.01	43.25
62	2	0	0.52	−9.74	3.75	0.45	41.06
62	2	1	27.02	−6.66	18.38	0.01	42.30
62	2	2	3.84	−10.69	5.59	0.02	42.66
62	3	0	−1.27	−9.56	2.03	0.40	28.55
62	3	1	27.69	−6.56	18.83	0.01	25.17
62	3	2	3.98	−10.56	5.71	0.01	29.94
62	4	0	−1.53	−10.08	2.18	0.41	12.89
62	4	1	27.07	−6.90	18.29	0.01	12.27
62	4	2	4.11	−10.58	5.63	0.02	9.47
171	1	0	0.98	−10.02	3.23	0.67	58.4
171	1	1	26.79	−6.95	18.37	0.01	52.58
171	1	2	7.12	−10.67	6.37	0.01	55.63
171	2	0	−2.0	−9.99	2.87	0.54	64.74
171	2	1	25.34	−7.08	17.98	0.02	69.87
171	2	2	6.86	−4.01	6.20	0.02	62.72
171	3	0	0.79	−10.11	3.02	0.46	53.66
171	3	1	27.01	−6.85	18.46	0.02	55.98
171	3	2	6.86	−10.59	6.11	0.02	56.56
364	1	0	4.44	−8.60	5.19	1.43	165.61
364	1	1	27.93	−6.76	19.27	0.02	171.67
364	1	2	0.04	−10.82	5.85	0.02	174.16
364	2	0	0.56	−9.65	3.55	0.65	113.62
364	2	1	30.70	−6.98	18.89	0.01	110.54
364	2	2	−0.28	−10.92	5.97	0.01	110.18
364 monomers	1	0	−6.67	−11.46	0.49	0.15	–
364 monomers	1	1	23.57	−7.12	16.55	0.15	–
364 monomers	1	2	−0.28	−12.02	5.99	0.15	–

[a] Energies are per monomer in kcal/mol. Nonbonded energy is the sum of the Lennard-Jones and Coulomb interactions. Bond angle energy is a contribution due to the deviations of valence angles from their equilibrium values. Bond energy is the contribution due to the stretching of chemical bonds. During MD runs, bond lengths were fixed by means of the SHAKE algorithm, with allowed deviations of 0.01 Å. Step 0, energy minimization; step 1, 100 ps annealing with short 4 Å cutoff at 1000 K; step 2, after 100 ps of MD with the 9 Å cutoff at 300 K. Notice that values at the end of steps 1 and 2 are the averaged values over the last 1000 steps of the molecular dynamics run. End-to-end distances are measured as the distance between the first and last hydrogens. The last three lines correspond to the liquid of 364 styrene monomers.

vector, and $f_j(q)$ is the atomic scattering factor for atom j.[33] The periodic box restricts the scattering intensity calculations to values of the scattering vector $\vec{q} = (2\pi/b)(n_x,n_y,n_z)$, where b is the box size and n_x, n_y, and n_z are integers. We assume that our amorphous structures are isotropic, and, therefore, calculate intensity as a function of the magnitude of the scattering vector by averaging $I(\vec{q})$ over scattering vectors with the same magnitudes.

Figures 7−9 show the scattering curves for the 62-mer, 171-mer, and 364-mer structures, respectively. Results are shown for the one configuration immediately after energy minimization (thick solid lines) and for each of the different configurations after 100 ps of MD annealing at 1000 K. The scattering patterns after 1000 K annealing show peaks observed experimentally at q values of 1.4 and 3.1 Å^{-1},[14,16,17,32] as well as the onset of the "polymerization" peak at approximately 0.75 Å^{-1}. No residual lattice periodicity is evident.

Figures 10−15 show the X-ray scattering patterns obtained at 300 K. The thin lines are the results for individual structures averaged over the last 100 ps of the MD run, while thick lines represent their averaged values. Although experimentally observed peaks at 0.75, 1.4, and 3.0 Å^{-1} are present on all the simulated curves at the same or nearly the same q values, it is evident that substantial quantitative differences exist in peak widths and heights. The low q values at 1.4 and 0.75 Å^{-1} correspond to the main and "polymerization" peaks, respectively. At higher q values, the scattering patterns from individual simulations are almost identical. Experiments have shown that X-ray scattering in region of low q, which arises mostly from scattering of atoms on different repeat units, was found to be sensitive to the sample annealing history and tacticity.[14,16] Thus, scattering in this range is especially sensitive to intermolecular packing and structural relaxations.[14]

The experimental X-ray scattering data from different sources are presented using different intensity scales. Therefore, only relative intensities from our simulated scattering patterns can be compared to the experimental results. Figures 16 and 17 present the ratio of scattering intensities at the different maximum peak heights to the peak maximum at approximately 2.9 Å^{-1}, and the experimental ratios.[14,32] Contrary to the results for the peaks at approximately 0.75 and 1.4 Å^{-1}, the relative intensity of the peak near 2.9 Å^{-1} shows little variation among the structures of different size and with different preparation histories. We find that the calculated intensities compare reasonably well with the experimental values. Substantial scatter in the data at the lower q values, corresponding to the main and "polymerization" peaks, reveals differences in intermolecular packing between different realizations of the model amorphous polystyrene structure.

Figure 18 shows the relative intensities at the maximum peak heights associated with the "polymerization" (circles) and main (squares) peaks, observed in our simulations as a function of system size and for two different annealing histories: sets A (filled symbols) and B (open symbols). Substantial deviations between the structures of the same size preclude determination of a statistically significant difference between the structures from sets A and B. However, the average values for the "polymerization" peak show systematic differ-

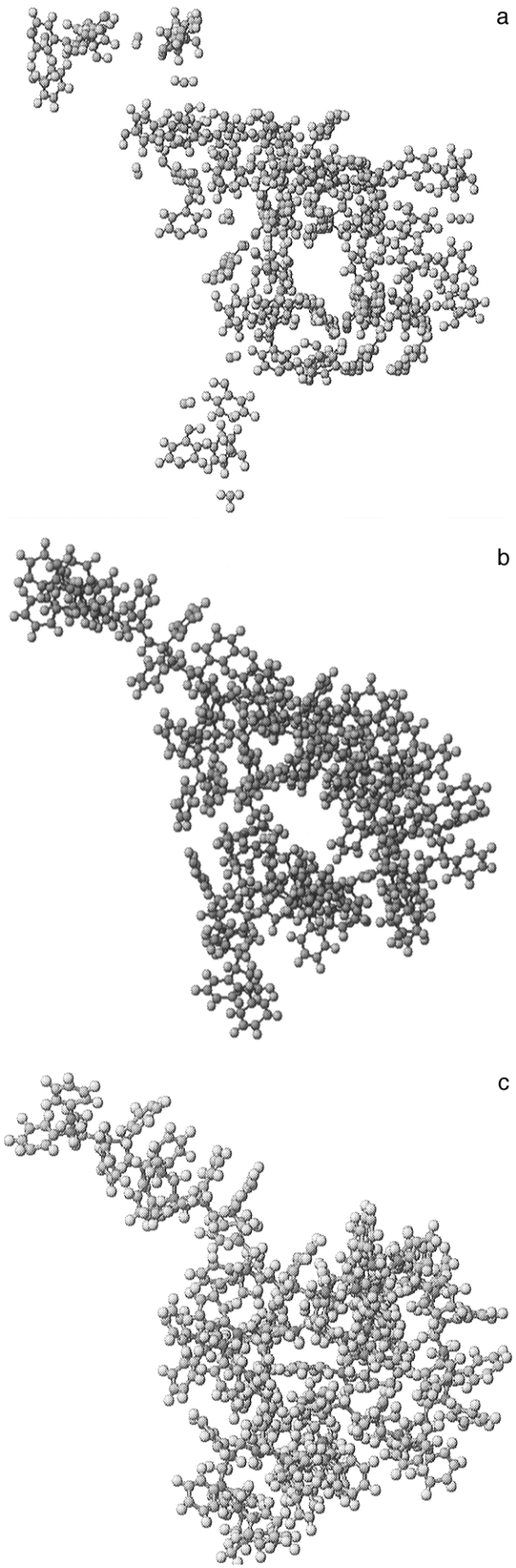

Figure 6. (a) Configuration of the 62-mer chain after lattice chain "decoration". (b) Same as in (a) after potential energy minimization. (c) Same as in (a) and (b) after 100 ps MD run at 1000 K.

Table 2. Population of the Different Conformational States for the Backbone C−C Bonds[a]

no. of monomers	g^-	t	g^+
62	0.22(0.05)	0.55(0.03)	0.23(0.03)
171	0.17(0.03)	0.63(0.03)	0.20(0.02)
364	0.20(0.03)	0.61(0.02)	0.19(0.03)

[a] Averaged over structures of the same size during the 100 ps MD run at 100 ps at 300 K. Numbers in parentheses represent deviations between structures of the same size.

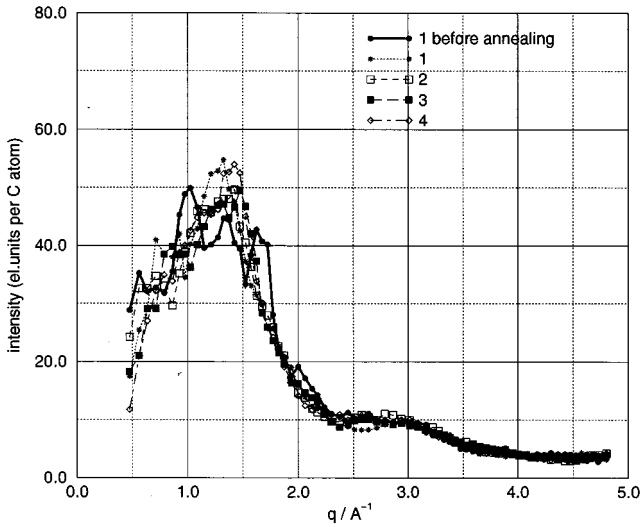

Figure 7. X-ray scattering intensities for 62-mers before and after high-temperature annealing. Thick solid line shows one of the structures immediately after energy minimization, illustrating the lattice scattering pattern. Thin lines represent 62-mer structures after 1000 K annealing.

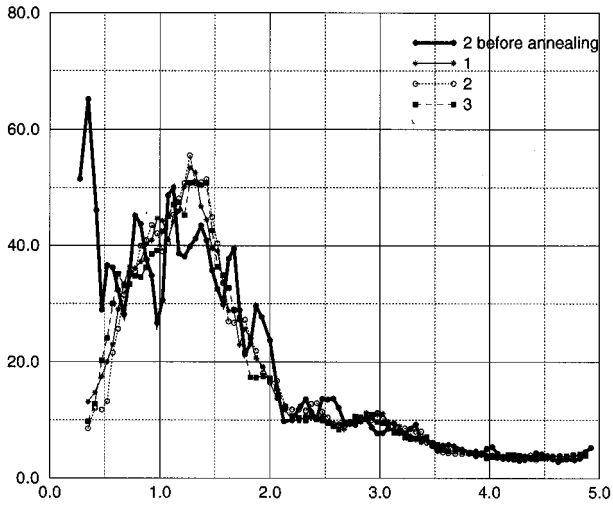

Figure 8. X-ray scattering intensities for 171-mers before and after high-temperature annealing. Thick solid line shows one of the structures immediately after energy minimization, illustrating the lattice scattering pattern. Thin lines represent 62-mer structures after 1000 K annealing.

ences between sampling histories. The average relative intensity for the largest structure is approximately 3.6. This value is higher than the experimental values of 2.64 (ref 32) and 2.85 (ref 14) at 293 K, but lower than 3.84 (ref 14) at 523 K.

We note, however, that these experimental results were obtained for polymers with different tacticities and densities. It is reasonable to expect discrepancies between the simulation results and the experimental scattering intensities due to the approximate nature of the interaction potentials used in the simulations. This may account for the overestimated relative intensity of

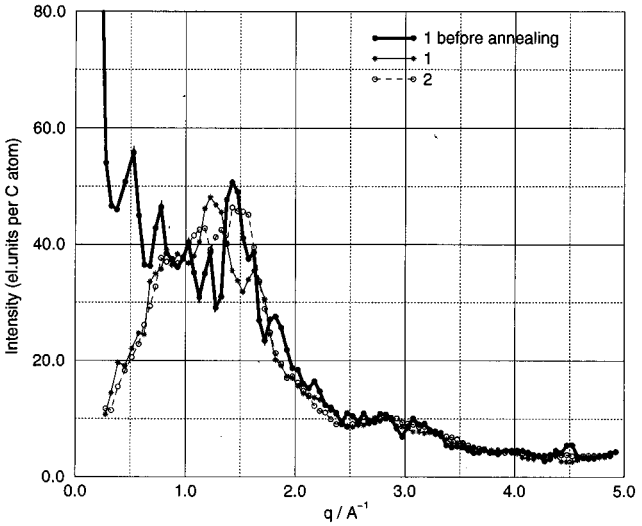

Figure 9. X-ray scattering intensities for 364-mers before and after high-temperature annealing. Thick solid line shows one of the structures immediately after energy minimization, illustrating the lattice scattering pattern. Thin lines represent 364-mer structures after 1000 K annealing.

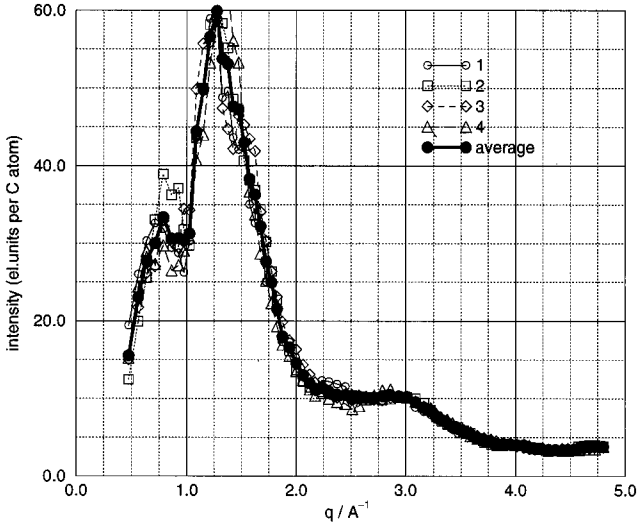

Figure 10. X-ray scattering patterns for four 62-mer structures of set A at the end of the 300 K run.

the "polymerization" peak, but not for the wide range of relative intensities obtained for different structures of the same size, or for different average values for the small and large structures.

The variation in relative scattering intensities for different structures of the same size is not unexpected. Rather, it is an indication that these structures represent different possible microscopic realizations of the macroscopic glassy polystyrene structure. It follows, therefore, that our individual structures are not large enough to represent all possible structural motifs present in the macroscopic glass.

As seen in Figure 18 and in the corresponding X-ray scattering patterns (Figures 10−15), the 62-mer structures are statistically distinct from the larger ones. These differences can be traced to a system size effect in the algorithm that apparently has gone unnoticed in previous simulation studies. In calculating electrostatic interactions, a residue-based cutoff is often employed.[5,30] Polystyrene has a rather bulky residue, which is taken to be the entire styrene monomer. Thus, for a cutoff in nonbonded interactions of 9 Å, a residue just inside this distance from a reference point of interest includes atoms that can be as far as 14 Å from the reference

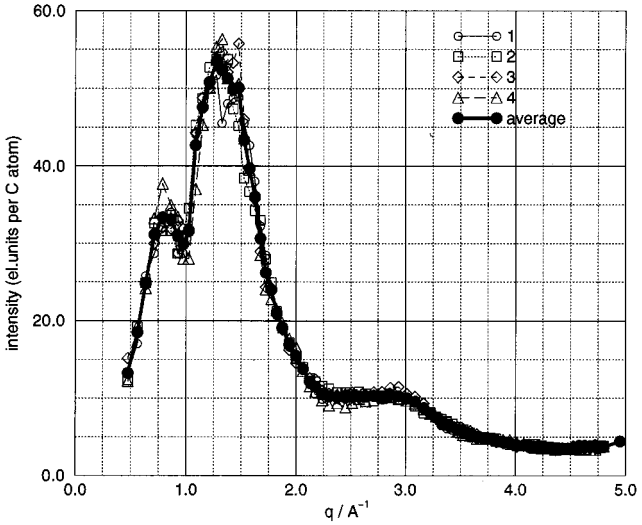

Figure 11. X-ray scattering patterns for four 62-mers of set B at the end of the 300 K run.

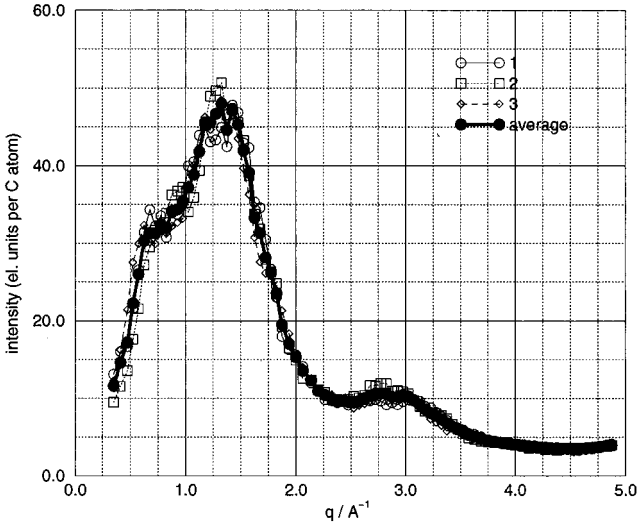

Figure 12. X-ray scattering patterns for three 171-mers of set A at the end of the 300 K run.

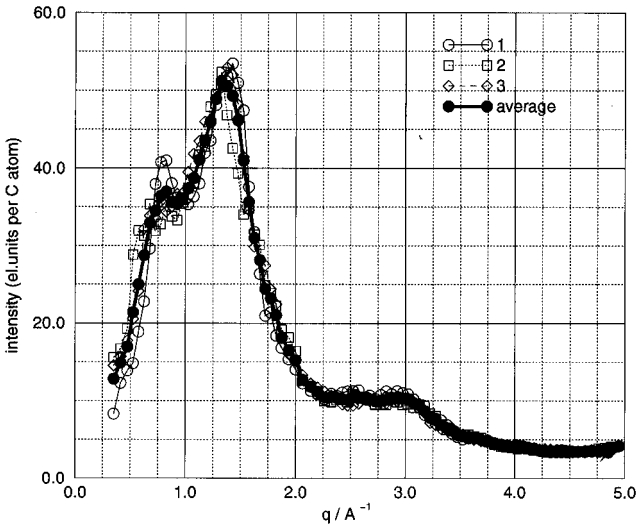

Figure 13. X-ray scattering patterns for three 171-mers of set B at the end of the 300 K run.

point. Consequently, applying the nearest image convention for box sizes less than twice this distance will lead to splitting this residue between different periodic boxes and, thus, generation of an artificial dipole. This effect occurs for all polystyrene structures in a periodic

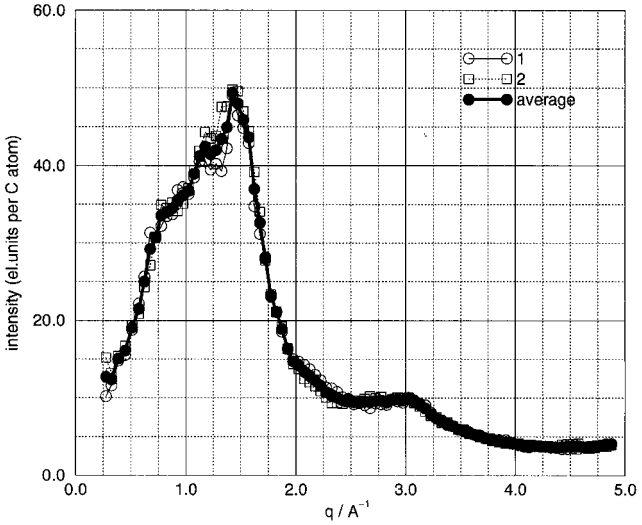

Figure 14. X-ray scattering patterns for two 364-mers of set A at the end of the 300 K run.

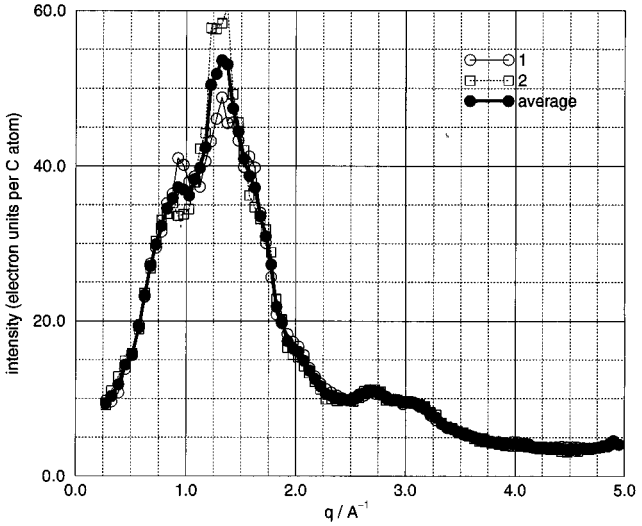

Figure 15. X-ray scattering patterns for two 364-mers of set B at the end of the 300 K run.

box less than 28 Å on a side. Our 62-mer structures are in periodic boxes 21.75 Å on a side, while the 171-mer and 364-mer structures are in much larger boxes: 30.625 and 39.15 Å on a side, respectively. Our algorithm for generating amorphous polymer structures enables efficient construction of structures larger than this critical size and thus avoids this box size artifact. Details of system size effects on other properties of polystyrene will be the subject of a forthcoming paper.[34]

V. Conclusions

We have presented a new technique for generating atomistic model structures of amorphous polymers that guarantees Gaussian chain statistics, allows specification of chain tacticity and monomer sequence, and at the same time avoids severe atomic overlaps in initial stages of preparation. We have also shown that the polymer chain on the completely occupied lattice is Gaussian with chain statistics equivalent to the non-reversing random walk on a cubic lattice. A single chain on the cubic lattice with periodic boundary conditions obeys the same statistics as shorter chains in multiple chain systems.[10]

The technique is robust and, therefore, enables the generation of polymers containing complex monomers. Moreover, large models of atactic polystyrene can be

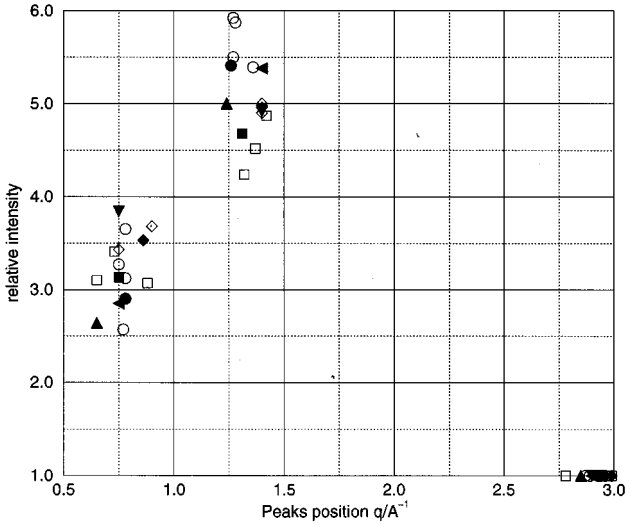

Figure 16. Peak positions and intensities, normalized by the peak intensity at approximately 2.9 Å^{-1} for set A. Open symbols: ○, 62-mers; □, 171-mers; ◇, 364-mers. Corresponding filled symbols represent values for average intensity curves. Experimental values: △, ref 32; ▽, ref 14 at 293 K; ▽, ref 14 at 523 K.

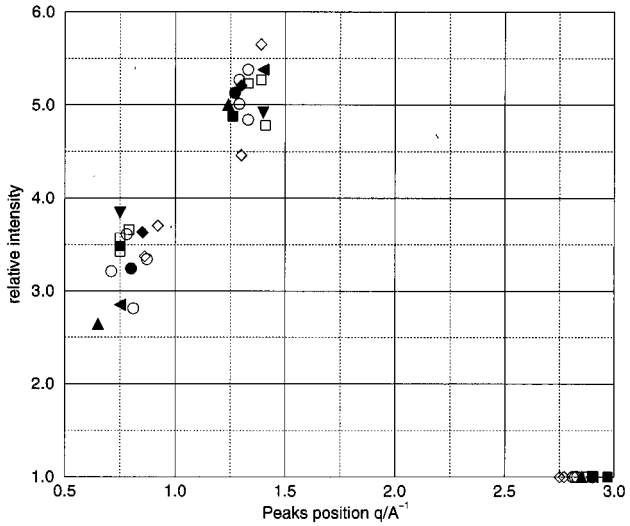

Figure 17. Peak positions and intensities, normalized by the peak intensity at approximately 2.9 Å^{-1} for set B. Open symbols: ○, 62-mers; □, 171 mers; ◇, 364-mers. Corresponding filled symbols represent values for average intensity curves. Experimental values: △, ref 32; ▽, ref 14 at 293 K; ▽, ref 14 at 523 K.

produced within a reasonable amount of CPU time; for example, several large polystyrene structures can be generated overnight on an IBM RISC6000/590 workstation. Relatively short annealing times (approximately 100 ps) after energy minimization proved to be sufficient to eliminate any artificial lattice periodicity imposed on the system in the initial preparation stage. Nevertheless, further annealing was required to reproduce experimentally observed X-ray scattering patterns.

Although the qualitative features of experimental scattering curves were reproduced for all sample sizes, observed variations in the scattering patterns and their sensitivity to the system size lead us to conclude that structures even larger than the 364-mer studied here are required in order to realize truly representative polystyrene structures.

Acknowledgment. Financial support from Dow Chemical Co. and the Delaware Research Partnership

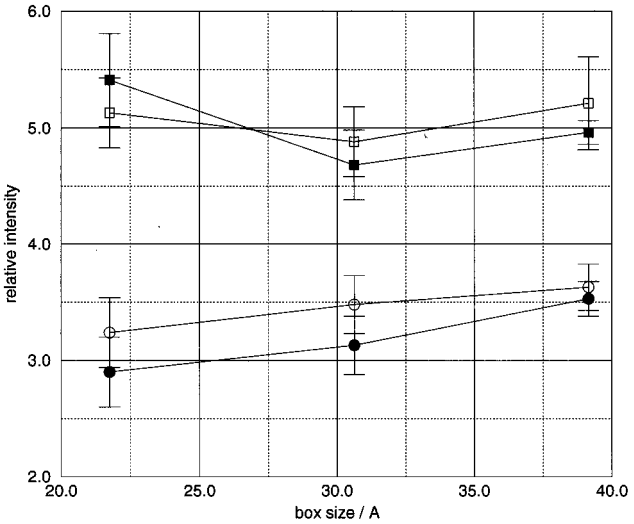

Figure 18. "Polymerization" (ca. 0.75 Å^{-1}) and main (ca. 1.4 Å^{-1}) peak intensities, normalized by the scattering intensity of the peak at ca. 2.9 Å^{-1} for all structures vs system size. □ Main peak; ○, "polymerization" peak. Filled symbols, set A; empty symbols, set B. Error bars show deviations for structures of the same size.

Fund is gratefully acknowledged. This research was conducted using the resources of the Cornell Theory Center, which receives major funding from the National Science Foundation and New York State, the Advanced Research Projects Agency, the National Institute of Health, IBM Corp., and other members of the Center's Corporate Research Institute.

References and Notes

(1) Hansen, J. P.; McDonald, I. R. *Theory of Simple Liquids*; Academic Press: New York, 1986.
(2) Allen, M. P; Tildesley, D. J. *Computer Simulation of Liquids*; Clarendon Press: Oxford, 1993.
(3) McKehnie, J. I; Brown, D.; Clarke, J. H. R. *Macromolecules* **1992**, *25*, 1562.
(4) Theodorou, D. N.; Suter, U. W. *Macromolecules* **1985**, *18*, 1467.
(5) Khare, R.; Paulaitis, M. E.; Lustig, S. R. *Macromolecules* **1993**, *26*, 7203.
(6) Flory, P. J. *Statistical Mechanics of Chain Molecules*; Hanser Publishers: New York, 1989.
(7) Rapold, R. F.; Suter, U. W. *Macromol. Theory Simul.* **1994**, *3*, 19.
(8) Hutnik, M.; Gentile, F. T.; Ludovice, P. J.; Suter, U. W.; Argon, A. S. *Macromolecules* **1991**, *24*, 5962.
(9) Ludovice, P. J.; Suter, U. W. In *Computational Modeling of Polymers*; Bicerano, J., Ed.; Marcel Dekker: New York, 1989.
(10) Pakula, T.; Geyler, S. *Macromolecules* **1987**, *20*, 679.
(11) Doi, M.; Edwards, S. F. *The Theory of Polymer Dynamics*; Clarendon Press: Oxford, 1994.
(12) Geyler, S.; Pakula, T.; Reiter, J. *J. Chem. Phys.* **1990**, *92*, 2676.
(13) Mondello, M.; Yang H.-J.; Furuya, H.; Roe, R.-J. *Macromolecules* **1994**, *27*, 2566.
(14) Mitchell, G. R.; Windle, A. H. *Polymer* **1984**, *25*, 906.
(15) Kanaya, K.; Kawaguch, T.; Kaji, K. *J. Non-Cryst. Solids* **1994**, *172*−174, 327.
(16) Song, H.-H.; Roe, R.-J. *Macromolecules* **1987**, *20*, 2723.
(17) Adams, R.; Balyuzi, H. H.; Burge, R. E. *J. Mater. Sci.* **1972**, *7*, 1249.
(18) Furuya, H.; Mondello, M.; Yang H.-J.; Roe, R.-J.; Erwin, R. W.; Han, C. C.; Smith, S. D *Macromolecules* **1994**, *27*, 5674.
(19) Pakula, T.; Geyler, S. *Macromolecules* **1988**, *21*, 1665.
(20) Gauger, A.; Pakula, T.; *Macromolecules* **1995**, *28*, 190.
(21) Binder, K. *Faraday Discuss.* **1994**, *98*, 97.
(22) Binder, K.; Deutsch, H.-P.; Micka, U.; Muller, M. *Nuclear Phys. B* **1995**, 27.
(23) Muller, M.; Binder, K. *Macromolecules* **1995**, *28*, 1825.
(24) Wolfgradt, M.; Baschnagel, J.; Binder, K. *J. Phys. II* **1995**, *5*, 1035.
(25) Verdier, P. H.; Stockmayer, W. H. *J. Chem. Phys.* **1962**, *36*, 227.
(26) Olaj, O. F.; Lantschauber, W. *Makromol. Chem., Rapid Commun.* **1982**, *3*, 847.
(27) Mansfeld, M. L. *J. Chem. Phys.* **1982**, *77*, 1554.
(28) Mom, V. *J. Comput. Chem.* **1981**, *2*, 446.
(29) Reiter, R. *Macromolecules* **1990**, *23*, 3811.
(30) Weiner, S. J.; Kollmann, P. A.; Case, D. A.; Singh, U. C.; Ghio, C.; Alagona, G.; Profeta, S.; Weiner, P. *J. Am. Chem. Soc.* **1984**, *106*, 765.
(31) Ryckaert, J. P.; Ciccoti, G.; Berendsen J. J. C. *J. Comput. Phys.* **1977**, *23*, 327.
(32) Schubach, H. R.; Nagy, E.; Heise, B. *Colloid Polym. Sci.* **1981**, *259*, 789.
(33) Macgillvary, C. H.; Rieck, G. D.; Lonsdale, K. *International Tables for X-ray Crystallography*; The Kynoch Press: Birmingham, England, 1968.
(34) Cuthbert, T.; Wagner, N. J.; Paulaitis M. E. *Macromolecules*. Submitted.

MA960071B